Sustainable Energy & Fuels

ROYAL SOCIETY OF CHEMISTRY

PAPER

View Article Online
View Journal | View Issue

Cite this: *Sustainable Energy Fuels*, 2025, **9**, 2355

Conversion of wood waste into nitrogen-doped graphite-like multiporous carbon with high specific surface area and electrical conductivity for high-voltage supercapacitors†

Shu-Sian Wang,‡[a] Chun-Han Hsu, ‡[b] Cheng-Ta Tsai,[a] Hong-Ping Lin, *[ac] Che-Wei Yan,[d] Jeng-Kuei Chang,[d] Tzu-Hsien Hsieh,[e] Cheng-Wei Huang[e] and Cheng-Hsien Lee[f]

A novel synthesis method is proposed for preparing nitrogen-doped graphite-like multiporous carbon (N-GMPC) from wood biochar using oyster shell powder as an activating agent without using inert gas. The proposed method is demonstrated using three different biochar precursors: *Acacia confusa*, *Leucaena leucocephala*, and a mixture of scrap wood. The N-GMPC derived from *Acacia confusa* exhibits a large specific surface area of 1638 $m^2\ g^{-1}$, a high nitrogen content of 4.2 wt%, and a good electrical conductivity of 9.37 $S\ cm^{-1}$. In addition, organic supercapacitor applications with 1.0 M $TEABF_4$/PC electrolyte demonstrate a specific capacitance of 129 $F\ g^{-1}$ and a capacitance retention rate of 90% in the high voltage range of 2.3 to 2.7 V after 30 000 cycles. In contrast, commercial porous carbon shows a capacitance retention rate of just 29% under equivalent conditions. Notably, the N-GMPC overcomes many limitations of traditional porous carbon materials in supercapacitors, such as an amorphous structure and poor conductivity, which hinder its rate performance and cycle life. Even without conductive additive (Super P), the N-GMPC maintains a similar performance. In other words, the N-GMPC has good intrinsic conductivity. In high-voltage electrolytes up to 4.0 V (1.0 M $SBPBF_4$/ADN), the N-GPMC maintains an impressive performance, with a specific capacitance of 164 $F\ g^{-1}$, an energy density of 61.19 W h kg^{-1}, a power density of 23.22 kW kg^{-1}, and a capacitance retention of 80% after 10 000 cycles. Overall, the synthesis strategy proposed in this study offers a novel pathway for deriving sustainable energy storage materials from natural waste biomass resources.

Received 17th November 2024
Accepted 18th March 2025

DOI: 10.1039/d4se01603c

rsc.li/sustainable-energy

1. Introduction

Taiwan generates approximately two million tons of agricultural waste annually, including rice straw, fallen fruits, and livestock manure.[1] In the past, this waste was mainly managed through composting, incineration, or on-site burial. However, with growing awareness of the need for environmental protection and resource sustainability, the requirement for more efficient waste management practices has attracted increasing attention.[1,2] One promising approach is to convert agricultural waste into biochar through biomass pyrolysis in an oxygen-limited or oxygen-free environment.[2] Biochar has many advantageous properties, including high stability, good porosity, and a low production cost.[2–5] Consequently, it has been the subject of intense research in recent years, particularly regarding its potential use in industrial and energy applications.[5]

Biochar has diverse applications in energy storage, catalysis, absorbance, and soil improvement.[3–6] Among these applications, its potential as an electrode material in supercapacitors or batteries has attracted particular interest. However, the inherent characteristics of biochar do not fully meet the stringent requirements for supercapacitor electrodes, such as high conductivity and specific surface areas.[7] Several techniques have been developed to address these challenges, including activation, heteroatom doping, and graphitization.[7,8] While these methods improve the performance of biochar in advanced

[a]*Department of Chemistry, National Cheng Kung University, No. 1 University Road, Tainan City 70101, Taiwan. E-mail: hplin@mail.ncku.edu.tw*

[b]*General Education Center, National Tainan Junior College of Nursing, No. 78, Sec. 2, Minzu Road, Tainan City 70043, Taiwan*

[c]*Hierarchical Green-Energy Materials (Hi-GEM) Research Center, National Cheng Kung University, No. 1 University Road, Tainan City 70101, Taiwan*

[d]*Department of Materials Science and Engineering, National Yang Ming Chiao Tung University, 1001 Daxue Road, Hsinchu City 30010, Taiwan*

[e]*Green Technology Research Institute, CPC Corporation, No. 2, Zuonan Rd, Kaohsiung City 81126, Taiwan*

[f]*FanC Recycling International Ltd, 1F, No. 560, Ziyou 3rd Rd, Kaohsiung City 81364, Taiwan*

† Electronic supplementary information (ESI) available. See DOI: https://doi.org/10.1039/d4se01603c

‡ Shu-Sian Wang and Chun-Han Hsu are equal contributions.

energy storage systems, continued innovation in biochar modification is still required to meet the ever-increasing demands for higher energy density and longer cycle lives in modern technological applications.

Porous carbon materials have high specific surface areas and well-developed porosity and thus hold exceptional promise for supercapacitor applications, which require rapid ion adsorption and desorption.[7,8] The ability to produce high-quality porous carbon from waste biomass aligns with the principles of waste valorization and environmental sustainability.[9–11] However, traditional porous carbon materials have poor electrical conductivity, which restricts their effectiveness in high-current applications.[12] Moreover, the structure of traditional activated carbon is predominantly composed of amorphous carbon, which diminishes the conductivity and adversely affects the cycle life during rapid charge–discharge cycles.[13–15]

Although the electrical performance of porous carbon materials can be improved by doping the surface with heteroatoms and enhancing the graphitization degree of the material,[16–19] increasing the degree of graphitization typically requires the use of high temperatures (greater than 1000 °C). Such high temperatures not only prompt a collapse of the carbon pores, which hinders the doping effect but also incurs a high energy cost.[20–23] Consequently, enhancing the performance of porous carbon materials in a sustainable and low-cost manner in a one-step synthesis process remains a significant challenge.

To address this challenge, this study proposes a novel chemical synthesis method based on physical and chemical activation to synthesize porous carbon materials using biochar. The proposed method allows the simultaneous control of the porosity, heteroatom doping, and degree of graphitization and facilitates the one-step synthesis of nitrogen-doped graphite-like multiporous carbon (N-GMPC) with a high specific surface area and good conductivity. Furthermore, the study replaces calcium carbonate reagents with oyster shells, incorporating the concept of waste reutilization and reducing chemical reagents. In organic supercapacitor applications, the N-GMPC demonstrates synergistic effects due to its optimized pore characteristics, nitrogen content, and degree of graphitization. The experimental results show that the performance metrics of the synthesized N-GMPC material surpass those of commercial porous carbon.

2. Materials and methods

2.1. Materials

Biochar was produced from commercial industrial waste using a top-lift updraft (TLUD) carbonization furnace by FanC Recycling International Ltd (Taiwan).[24] Potassium hydroxide (KOH) and hydrochloric acid (HCl) were purchased from He Cheng Chemical Co. Ltd (Taiwan). Melamine (99%) was sourced from Thermo Scientific Chemicals (USA). Oyster shell powder (OSP) was obtained from Taiwan Sugar Co. Ltd (Taiwan). Commercial porous carbon (CPC) was acquired from Osaka Gas Chemicals Co. Ltd (Japan). The properties of the CPC are shown in Fig. S1 and Table S1 in the ESI.†

2.2. Preparation of N-GMPC *via* simple one-step blending method

Biochar was derived from *Acacia confusa*, *Leucaena leucocephala*, and general leftover waste wood generated by a wood processing factory in Taiwan. A mixture of 20 g of biochar, 6 g of melamine, and 16 g of KOH was uniformly blended in an aqueous solution and evaporated to obtain a solid sample. Subsequently, 60 g of OSP and the solid sample were placed sequentially in an alumina crucible for activation in a muffle furnace without introducing inert gas. The activation process consisted of two stages. In the first stage, the temperature was raised to 550 °C and held for 4 h. Subsequently, it was increased to 900 °C and maintained for 10 h. The heating rate was set to 8 °C min^{-1} in both stages. After activation, the samples were collected and washed with 37 wt% hydrochloric acid and deionized water to remove residual activators and impurities. The final N-GMPC material was obtained by drying the washed samples at 100 °C.

2.3. Characterization of N-GMPC

The nitrogen adsorption–desorption isotherms were measured at −196 °C using a Micromeritics Tristar II 3020 analyzer. The Brunauer–Emmett–Teller (BET) model was employed to calculate the specific surface area of the materials. The pore size and volume were determined using the two-dimensional non-local density functional theory with heterogeneous surfaces (2D-NLDFT-HS) method. The morphology and microstructure of the samples were observed using a scanning electron microscope (SEM, HITACHI SU8010) and a high-resolution transmission electron microscope (HRTEM, JEOL JEM-2100F + Cs Corrector STEM). The crystalline properties were characterized by X-ray diffraction (XRD, Bruker D8 Advance) using Cu Kα radiation (40 kV, 25 mA, $\lambda = 1.5406$ Å). The average crystallite size was calculated using the Scherrer equation based on the XRD results. The structural features of the samples were analyzed using confocal Raman spectroscopy (Horiba iHR-550, wavelength 532 nm) and micro-Raman spectroscopy (Horiba Jobin Yvon/Labram HR, wavelength 325 nm). The chemical composition of the samples was examined by X-ray photoelectron spectroscopy (XPS, PHI VersaProbe 4) using Al Kα radiation. The elemental composition (C, H, O, and N) was determined using an elemental analyzer (Elementar Vario EL Cube). Finally, the electrical conductivity of the samples deposited on the separator membranes was measured with a four-point probe resistance meter (KeithLink LRS4-T).

2.4. Assembly and electrochemical measurement of symmetric supercapacitors

Active material (87 wt%), carbon black (Super P, 6.5 wt%), and polyvinylidene fluoride (PVDF) (6.5 wt%) were uniformly mixed and deposited onto glass fiber membranes (GF/D, Whatman) to serve as an electrode. Following the deposition process, the electrodes were dried at 100 °C for 12 h to facilitate the complete removal of any residual moisture and solvent. Each electrode had an effective area of 1.33 cm^2 and contained approximately 3 mg of active material. Two identical electrodes were

assembled with carbon-plated aluminum foil to construct a CR-2032 coin-cell supercapacitor. The assembly process was performed in a glovebox under an Ar atmosphere to ensure a clean, dry, and inert environment. The performance of the N-GMPC as an electrode material was evaluated using two organic phase electrolytes: commercial organic electrolyte 1.0 M $TEABF_4$/PC and high-voltage resistant electrolyte 1.0 M $SBPBF_4$/ADN.

Electrochemical characterization of the coin-cell supercapacitors was performed using a CHI6142C potentiostat (CH Instruments, USA). The evaluations included cyclic voltammetry (CV), galvanostatic charging–discharging (GCD), and electrochemical impedance spectroscopy (EIS). The CV measurements were conducted over the potential range of −2.7 to 2.7 V. The specific capacitance (F g^{-1}) was calculated as a function of the voltage using the equation $C = 2I/vm$, where I is the current (A), v is the scan rate (V s^{-1}), and m is the mass (g) of the carbon material in each electrode. The potential was scanned between 0 and 2.7 V for the GCD tests. The specific gravimetric capacitance of each electrode (F g^{-1}) was determined from the galvanostatic cycles using the equation $C = 2I/(\mathrm{dV\ dt^{-1}})\mathrm{m}$, where $\mathrm{dV\ dt^{-1}}$ is the slope of the discharge curve (V s^{-1}). The energy density (E) and power density (P) were calculated as $E = \mathrm{CV}^2/(8 \times 3.6)$ and $P = E/\Delta t$, respectively. The EIS measurements were performed over the frequency range of 10^5–10^{-2} Hz with a voltage amplitude of 5 mV.

2.5. Computational studies

Density functional theory (DFT) calculations were performed to examine the conductivity effects of nitrogen doping in the N-GMPC material. The biochar material was modeled using a coronene model. The N-GMPC was modeled by substituting two central carbon atoms in the coronene structure with nitrogen atoms. Both models were constructed using Gauss-View software. DFT calculations for the geometry optimization and electronic properties of the two materials were conducted using the Gaussian 09 software package. Geometry optimization, frequency analysis, and energy calculations for the studied molecules were performed using the Minnesota meta-exchange–correlation function M06-2X within the DFT framework. All the computations used the 6-31G (d,p) basis set.

3. Results and discussion

3.1. Synthesis and characterization of N-GMPC

As shown in the SEM images in Fig. 1a and b, the biochar (*Acacia confusa*) has a smooth surface, while the N-GMPC shows a well-developed 3D interconnected porous structure. The nitrogen adsorption–desorption isotherms in Fig. 1c show that the biochar exhibits type I characteristics, indicating that its pores are predominantly microporous. In contrast, the N-GMPC material exhibits type IV characteristics, which suggests that its structure consists of a combination of micropores and mesopores. The BET analysis results reveal that the biochar has a specific surface area of approximately 230 $m^2\ g^{-1}$, whereas that of the N-GMPC is significantly higher at 1638 $m^2\ g^{-1}$. The pore volume and average pore diameter of the N-GMPC material, as calculated using 2-DNLDFT-HS, are also substantially higher. In particular, the pore volume increases from 0.07 $cm^3\ g^{-1}$ in the biochar to 0.92 $cm^3\ g^{-1}$ in the N-GMPC, while the average pore diameter increases from 1.92 nm for the biochar to 2.89 nm for the N-GMPC. In other words, the proposed

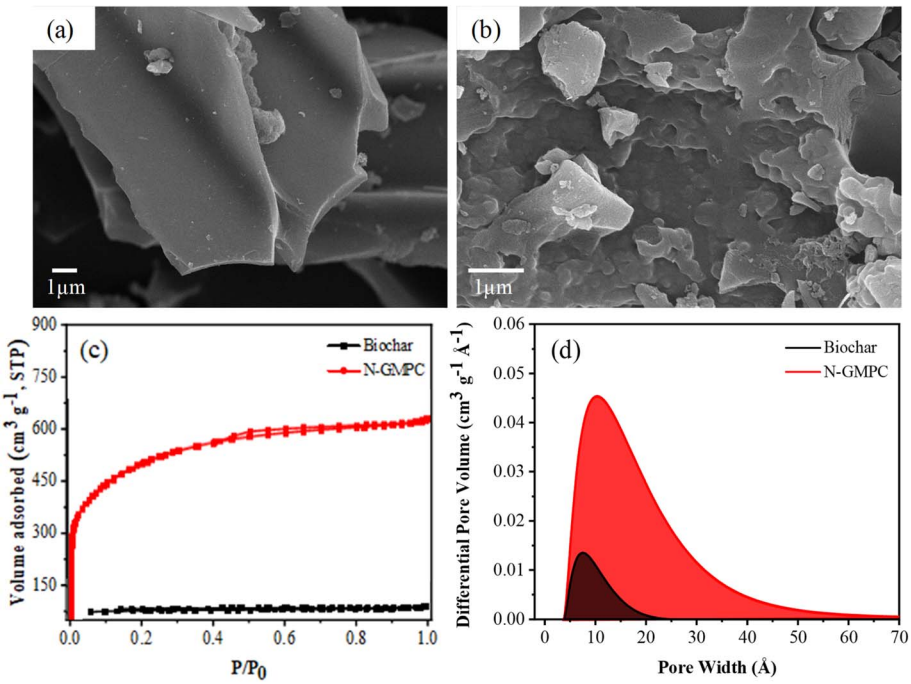

Fig. 1 SEM morphologies of (a) biochar (*Acacia confusa*) and (b) N-GMPC; and (c) N_2 adsorption–desorption isotherms and (d) pore size distribution curves of biochar and N-GMPC.

synthesis process not only enlarges the size of the existing pores but also creates new ones. These results are corroborated by the pore size distribution curves in Fig. 1d, which show that the N-GMPC material has a broader pore size distribution than that of the biochar.

The crystalline properties of the N-GMPC and biochar were determined using XRD analyses. The XRD patterns of graphitic carbon typically feature two characteristic peaks at $2\theta \approx 26°$ and $2\theta \approx 43°$, corresponding to the (002) and (100) crystal planes of graphite, respectively.[25] As shown in Fig. 2a and b, the biochar and N-GMPC materials exhibit notably different crystalline structures. In particular, the (002) and (100) diffraction peaks of biochar are broad and weak, indicating low crystallinity, while those of the N-GMPC are narrower and more distinct, suggesting improved crystallinity. To further evaluate the differences in the crystalline structures of the two materials, baseline correction was applied to eliminate the influence of high-intensity diffraction peaks at low angles. The resulting XRD patterns were individually fitted to the (100) peak of the carbon material, and the Scherrer equation was then employed to calculate the corresponding La value.[19] The fitting results of the (100) peak for the biochar and N-GMPC are shown in Fig. 2c and d, respectively. The N-GMPC exhibits a narrower full width at half maximum (FWHM) of the (100) peak (2.303°) and a higher La value (6.24 nm) than that of the biochar (FWHM: 5.070°, La value: 3.44 nm). These results confirm that the proposed synthesis route successfully enhances the degree of graphitization in the N-GMPC compared to the original biochar.

The graphitization of the activated N-GMPC material was further investigated by Raman spectroscopy using visible (532 nm) and ultraviolet (325 nm) light. As shown in Fig. 3a, the biochar and N-GMPC spectra exhibit prominent signals at 1350 and 1580 cm^{-1}, corresponding to the D and G bands of carbon materials, respectively.[26] Interestingly, both materials show similar R values (I_D/I_G), which indicates a similar degree of graphitization.[27] This result contradicts the XRD analysis but is consistent with the literature.[19] The discrepancy most likely arises because the increased specific surface area resulting from activation introduces more defects into the carbon material.[28,29] Additionally, incorporating nitrogen into the carbon structure further increases the defect level.[30] In other words, the R-value alone does not provide a fully objective measure of the degree of graphitization. Instead, it is necessary to analyze the intensity of the 2D band (2700 cm^{-1}) and verify it using ultraviolet Raman spectroscopy, which has a stronger incident light intensity.[31] As shown in Fig. 3a, the N-GMPC exhibits a stronger 2D band signal than the biochar. Furthermore, in the ultraviolet Raman spectra shown in Fig. 3b, the N-GMPC exhibits a lower R-value. These results confirm that the N-GMPC has a higher degree of graphitization than the biochar.

To further substantiate the difference in graphitization before and after activation, HRTEM was employed to observe the microstructures of the biochar and N-GMPC. The low-magnification images in Fig. 4a and e reveal significant differences between the two materials. In particular, the biochar has a dense, block-like structure, while the N-GMPC has a loose,

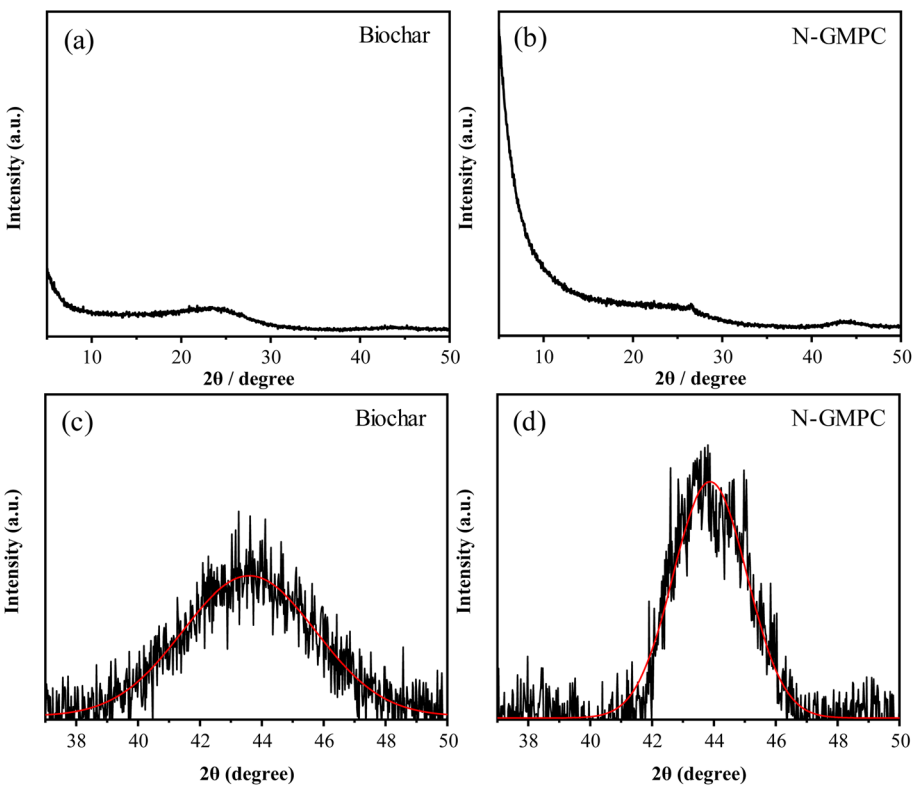

Fig. 2 XRD patterns of (a) biochar and (b) N-GMPC samples. High-resolution XRD (100) peaks of (c) biochar and (d) N-GMPC.

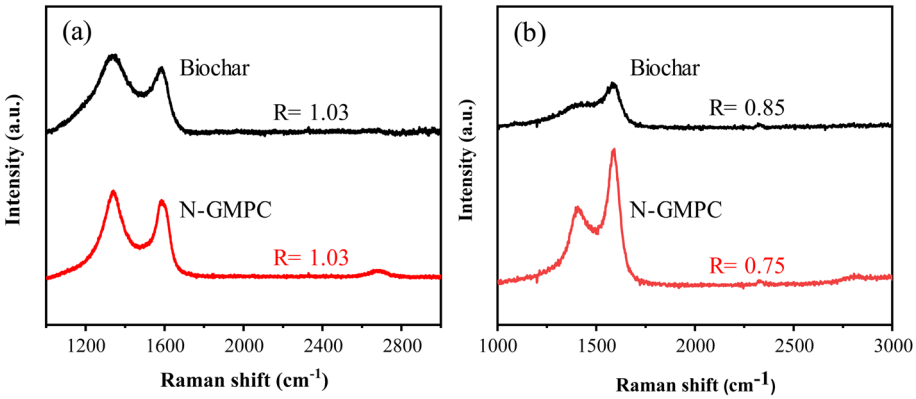

Fig. 3 (a) Visible Raman spectra and (excitation wavelength = 532 nm) and (b) UV Raman spectra (excitation wavelength = 325 nm) of the biochar and N-GMPC.

veil-like structure, which indicates better pore permeability. The high-magnification images in Fig. 4b–d and f–h show that both materials have graphite-like layered structures. However, the graphitized regions in the biochar are more localized, with the majority consisting of amorphous carbon structures. In contrast, the N-GMPC structure shows graphite lattice fringes with an interlayer spacing of 0.34 nm and more graphene structures.[32,33] These observations provide further evidence that the activation process proposed in this study effectively enhances the graphitization of the carbon material. The EDX mapping results in Fig. 4i–l reveal that the nitrogen doped into the carbon structure is uniformly distributed. Oxygen signals

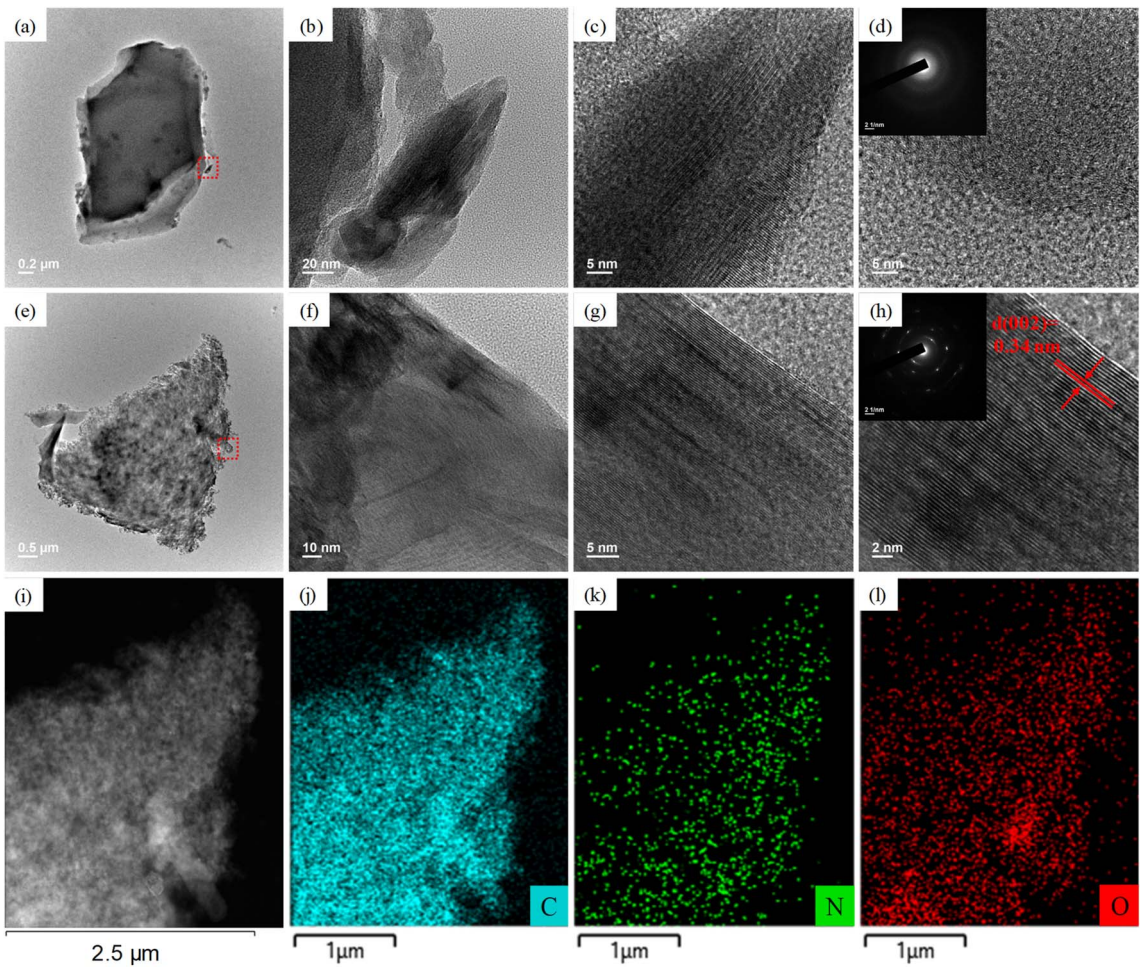

Fig. 4 HRTEM images of (a–d) biochar and (e–h) N-GMPC. (i–l) HRTEM EDX mapping results for N-GMPC.

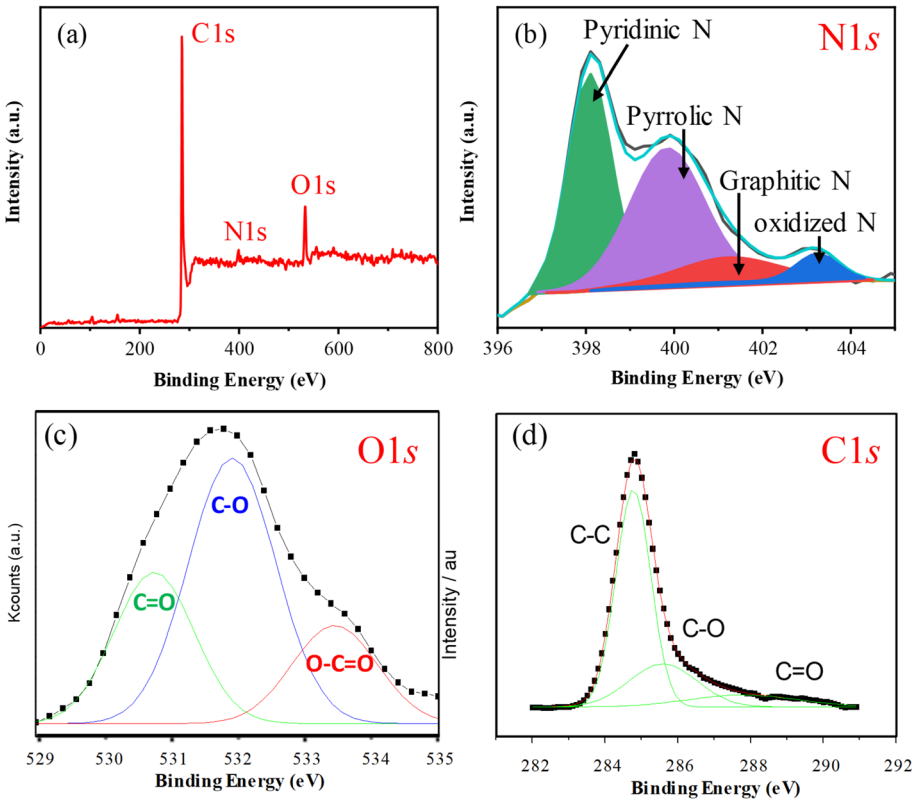

Fig. 5 (a) XPS survey spectrum, high-resolution (b) N 1s, (c) O 1s, and (d) C 1s spectra of the N-GMPC.

are also observed due to the use of biomass-derived carbon sources in synthesizing the N-GMPC material.[34]

Notably, the proposed synthesis process simultaneously enhances both the porosity and the graphitization of the carbon material as a result of the activation mechanism that occurs at temperatures above 900 °C. During this activation process, the activating agent (KOH) generates substances such as K_2O and K_2CO_3, which continue to react with the carbon.[35] Additionally, the potassium atoms produced during the reaction process penetrate between the carbon graphite microcrystals, facilitating their growth into long-range graphite structures.[36,37]

The elemental analyses revealed that the nitrogen content in the N-GMPC (4.2 wt%) was significantly higher than that in the biochar (1.1 wt%). The increase in nitrogen content is ascribed to the decomposition and N-doping reaction of the 3–5 wt% protein in the oyster shell. Thus, the results confirmed that the one-pot synthesis process proposed in this study effectively doped nitrogen into the carbon material during activation using oyster shell powder. The nitrogen bonding states in the N-GMPC were investigated *via* an XPS analysis. As shown in Fig. 5a, the XPS spectrum indicates the presence of only C, N, and O, with atomic percentages of 83.6%, 4.1%, and 9.5%, respectively. The absence of other metal signals indicates that the N-GMPC has a low ash content. In addition, the high-resolution N 1s spectrum shown in Fig. 5b reveals that the nitrogen-doped in the carbon structure primarily exists in the forms of pyridinic N (398.6 eV), pyrrolic N (400.5 eV), and graphitic N (401.4 eV), with only a small amount in the less stable form of oxidized N (403.3 eV).[38,39] Furthermore, as shown in the O 1s spectrum in Fig. 5c, the peak was deconvoluted into three components: a peak at approximately 531 eV corresponding to carbonyl groups (C=O) or ketonic functional groups; a peak at around 532 eV assigned to C–O bonds (indicative of hydroxyl (C–OH) or ether (C–O–C) linkages); and a peak at roughly 533.5 eV corresponding to carboxyl groups (O=C–OH).[39] These functional groups result from surface oxidation or functionalization of carbon and can significantly influence its electrochemical performance.[38–41] Further analysis of the C 1s XPS spectrum in Fig. 5d reveals that it can be deconvoluted into three main components: a peak at about 284.5 eV representing C–C bonds (graphitic carbon), which is the major constituent of the carbon-based material and corresponds to sp^2 carbon, as found in graphene or carbon nanotubes; a peak at approximately 285.5 eV corresponding to C–O bonds (indicative of hydroxyl or ether bonds); and a peak at around 288 eV corresponding to C=O bonds (carbonyl) or carboxyl groups (O=C–OH).[41] These components correlate well with the corresponding peaks in the O 1s spectrum, confirming the presence of various oxygen-containing functional groups on the surface. The C 1s spectrum clearly exhibits prominent C–O and C=O peaks, while the strong intensity of the C–C peak indicates that the carbon material largely retains its graphitic structure, despite some degree of surface oxidation leading to functionalization.

According to the literature, carbon materials with high graphitization and nitrogen doping have enhanced electrical conductivity.[30,42,43] Four-point probe measurements confirmed

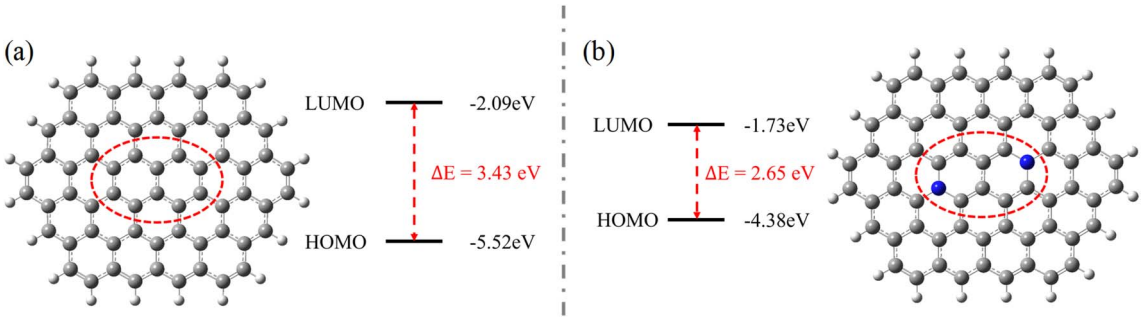

Fig. 6 Optimized structures and energy gaps of (a) undoped carbon material and (b) nitrogen-doped carbon material.

that the conductivity of N-GMPC (9.37 S cm^{-1}) was significantly higher than that of the biochar (0.11 S cm^{-1}). This enhanced electrical conductivity suggests that the N-GMPC has a reduced frontier orbital energy gap, that is, a lower energy difference between the lowest unoccupied molecular orbital (LUMO) and the highest occupied molecular orbital (HOMO). The DFT calculations shown in Fig. 6 confirm that the N-GMPC (Fig. 6b) has a smaller energy gap than the original biochar (Fig. 6a). This reduced energy gap implies a greater ease of charge transfer, which is directly associated with improved electrical conductivity.[44]

Overall, the structural and property analyses presented above confirm that the one-step synthesis method proposed in this study successfully produces nitrogen-doped graphite-like multiporous carbon materials with a range of exceptional characteristics, including a large specific surface area (1638 m^2 g^{-1}), high nitrogen content (4.2 wt%), and good electrical conductivity (9.37 S cm^{-1}).

To assess the versatility of the proposed synthesis process, two other common waste wood materials, *Leucaena leucocephala* and general scrap wood, consisting of various unknown wood types, all obtained from a wood processing factory, were selected for further study. The experimental results in Table 1 and Fig. 7 show that the synthesis process achieved a similar specific surface area, pore volume, nitrogen doping content, and improvement in the degree of graphitization for the

Table 1 Properties of N-GMPC materials derived from *Leucaena leucocephala* and leftover wood

Sample		S_{BET}/m^2 g^{-1}	Pore volume/cm^3 g^{-1}	N/wt%
Leucaena leucocephala	No activated	159	0.09	1.02
	Activated	1521	0.81	5.11
Leftover wood	No activated	173	0.11	0.83
	Activated	1646	0.86	3.74

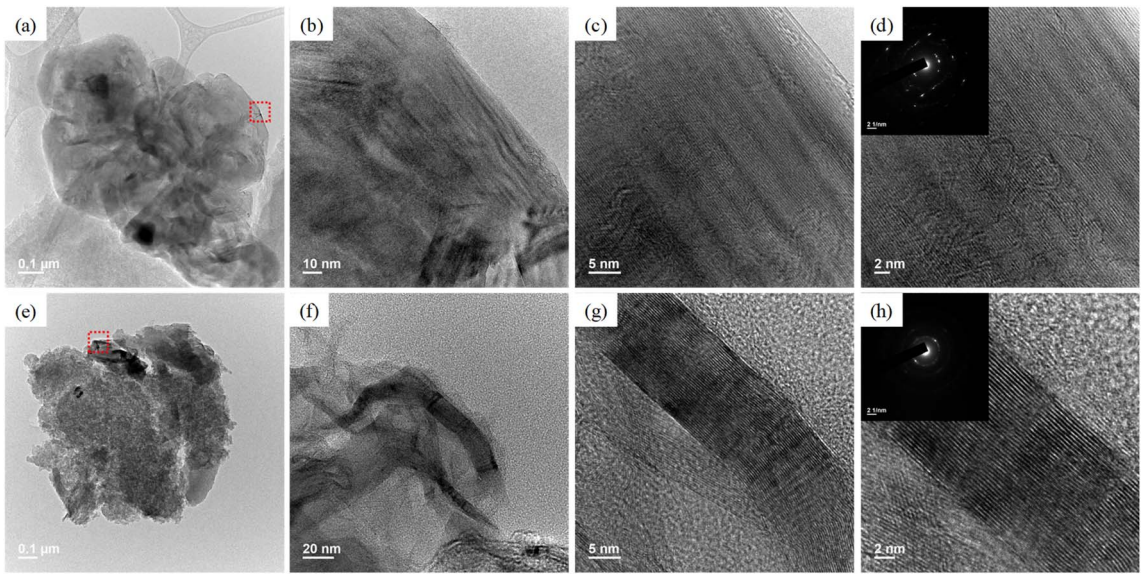

Fig. 7 HRTEM images of N-GMPC materials derived from (a–d) *Leucaena leucocephala* and (e–h) leftover wood.

original *Acacia confusa* source. Long-range graphite microcrystal structures are observed in the HRTEM images of both carbon sources (Fig. 7). In other words, the proposed synthesis process has good general applicability across various carbon sources.

3.2. Application of N-GMPC to supercapacitors

At a low scan rate (2 mV s^{-1}), the CV curves of the synthesized N-GMPC and CPC exhibited quasi-rectangular shapes, indicating a good electrical double-layer charge storage behavior (Fig. S2†). The similarity in the CV curve areas suggests that the two materials have comparable specific capacitances (CPC: 131 F g^{-1}, N-GMPC: 129 F g^{-1}). At a high scan rate (200 mV s^{-1}), the CV curve of the CPC material shows pronounced redox peaks and a small degree of distortion, as shown in Fig. 8a. In other words, the charge–discharge performance of the CPC is less stable than that of the N-GMPC at high scan rates. Consequently, the N-GMPC has a higher electrode rate capability (CPC: 70.2%, N-GMPC: 72.1%). Fig. 8b shows the EIS spectra of the CPC and N-GMPC. The combined series resistance (Rs) of the N-GMPC is smaller than that of the CPC (3.34 Ω, N-GMPC: 2.74 Ω) because of its high nitrogen content and well-developed graphite microcrystalline structure. Due to its superior conductivity, the N-GMPC material also has a lower charge-transfer resistance (R_{ct}) than the CPC in the high-frequency region (CPC: 3.36 Ω, N-GMPC: 1.13 Ω).[45] In the low-frequency region, both materials show a straight line with a steep slope, suggesting low ion diffusion/transport resistance or the Warburg element (W), both of which are associated with good electrical double-layer behavior.[46,47]

As shown in Fig. 8c, at a low current density (1 mA cm^{-2}), the GCD curves of N-GMPC and CPC both have a regular triangular shape. This result is consistent with the CV findings and indicates an ideal electrical double-layer charge storage mechanism. At a high current density (20 mA cm^{-2}), the N-GMPC demonstrates a longer charge–discharge duration than that of the CPC, as shown in Fig. 8d. This suggests that the N-GMPC has a higher specific capacitance than the CPC at high current densities. The superior pore structure and excellent conductivity of the N-GMPC result in a smaller IR drop (CPC: 0.291 V, N-GMPC: 0.222 V), which enables it to maintain a higher capacitance and better rate performance.[47–49]

To further substantiate the superior conductivity of N-GMPC, its performance in supercapacitor applications was investigated without adding the carbon black.[50,51] As shown in Fig. 9, even without this conductive additive, the N-GMPC still

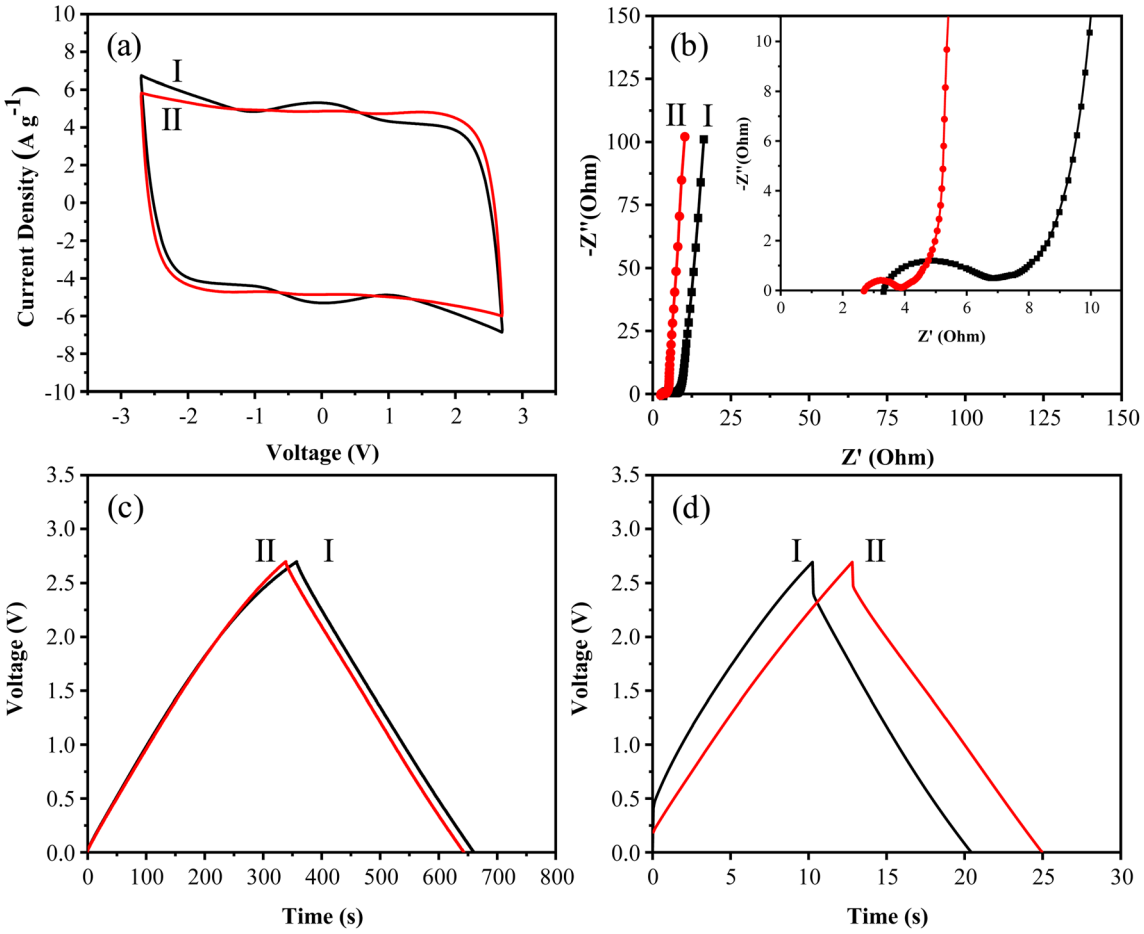

Fig. 8 Electrochemical performance of CPC (I) and N-GMPC (II) symmetric supercapacitors in 1.0 M $TEABF_4$/PC electrolyte. (a) CV curves at a scan rate of 200 mV s^{-1}. (b) EIS spectra. (c) GCD curves at a current density of 1 mA cm^{-2}. (d) GCD curves at a current density of 20 mA cm^{-2}.

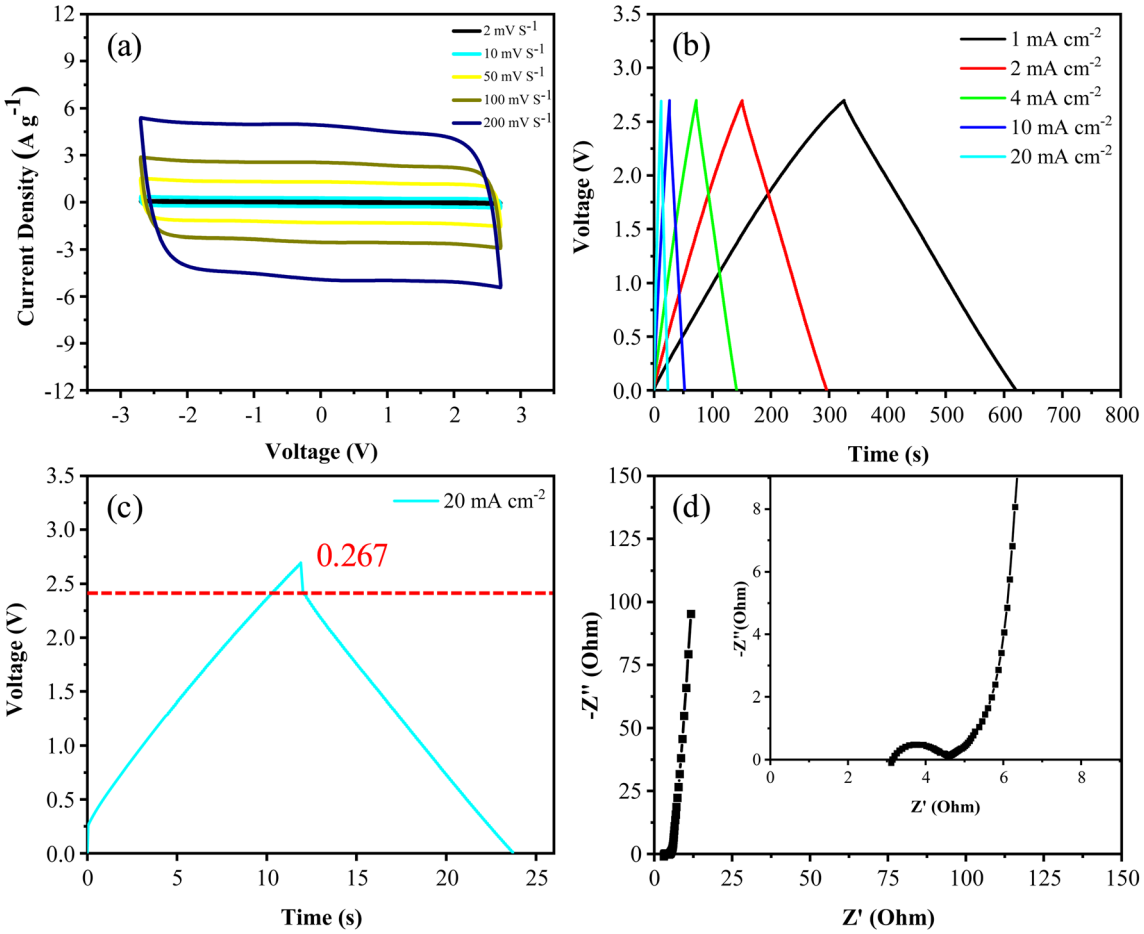

Fig. 9 Electrochemical performance of N-GMPC without conductive additive. (a) CV curves, (b) GCD curves, (c) GCD at 20 mA cm^{-2}, and (d) EIS spectra.

maintains a high specific capacitance (123 F g^{-1}) and electrode rate performance (72.3%), along with only a small IR drop (0.267 V) and low impedance (R_s: 3.14 Ω, R_{ct}: 1.46 Ω).

The energy density and power density are important indicators of the performance of energy storage devices. In the Ragone plot shown in Fig. 10a, the N-GMPC and CPC materials exhibit similar energy densities (N-GMPC: 25.2 W h kg^{-1}, CPC: 25.1 W h kg^{-1}) at low power densities (N-GMPC: 0.597 kW kg^{-1}, CPC: 0.597 kW kg^{-1}). However, at high power densities (N-GMPC: 11.9 kW kg^{-1}, CPC: 11.9 kW kg^{-1}), the N-GMPC has a higher energy density compared to the CPC (N-GMPC: 20.5 W h kg^{-1}, CPC: 16.8 W h kg^{-1}). The superior rate performance of N-GMPC can be attributed to two main factors.[52,53] First, during high current density charge–discharge processes,

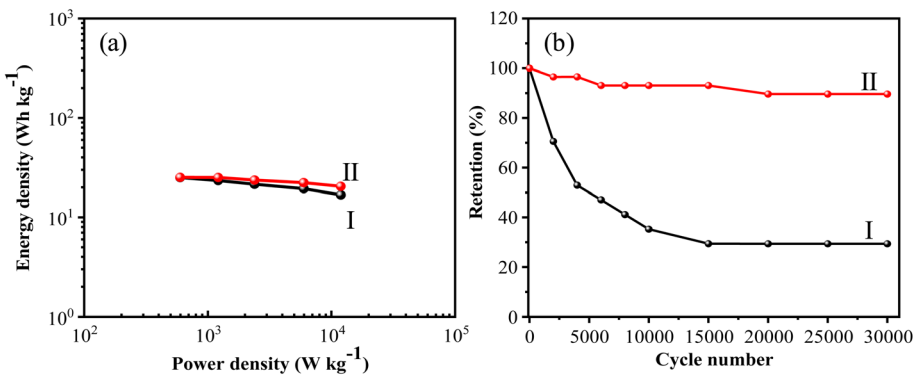

Fig. 10 (a) Ragone plots and (b) cycling stability of CPC (I) and N-GMPC (II) during 30 000 charge–discharge cycles at a current density of 10 mA cm^{-2} (approximately 4.4 A g^{-1}).

the electrons in the N-GMPC material travel along its rich graphite microcrystalline structure to the surface of some of the pores, allowing these graphite-surrounded pores to store charge more efficiently. Second, the nitrogen doping of the N-GMPC structure enhances its conductivity and reduces the losses caused by the IR drop at high current densities.

To further examine the difference in the cycle lives between N-GMPC and CPC, both materials were tested at a high current density of 10 mA cm^{-2} (approximately 4.4 A g^{-1}) in the high voltage range of 2.3 to 2.7 V for 30 000 cycles. It is noted that this high voltage range is critical in practical applications, as capacitors often experience significant performance degradation during rapid charge–discharge cycles at such voltages. As shown in Fig. 10b, even after 30 000 cycles, N-GMPC maintains a 90% capacitance retention rate. In contrast, the capacitance retention rate of CDC drops to 70% after just 2000 cycles and falls dramatically to 29% after 30 000 cycles.

The significant difference in the cycle life between the two materials stems from their distinct structural and compositional characteristics. N-GMPC has a significantly higher nitrogen content than CPC (N-GMPC: 4.24 wt%, CPC: 0.69 wt%), and properly structured nitrogen doping effectively suppresses side reactions in the electrolyte or electrode during charge–discharge processes, thus extending the cycle life of supercapacitors.[54,55] Furthermore, the HRTEM images in Fig. S3† show that the CPC mainly consists of a disordered carbon framework, compared to the ordered structure in N-GMPC (Fig. 4e–h). This disordered carbon framework induces irreversible side reactions of the electrolyte or internal oxygen groups in the carbon material during charge–discharge processes and thus significantly impairs the cycle life performance of supercapacitors.[19,56]

3.3. Application of N-GMPC to high-voltage supercapacitors

Since the power density and energy density of supercapacitors are both related to the square of the operating voltage window ($E = 1/2\ CV^2$, where C is the capacitance and V is the operating voltage window; $P = E\ t^{-1}$, where t is time), using an electrolyte with a larger operating voltage window can effectively enhance the energy and power densities of supercapacitors.[57] Supercapacitors generally exhibit low energy density under high voltage conditions. Thus, to examine the robustness of the synthesized N-GMPC as an electrode material, further charge–discharge tests were conducted in a voltage-resistant electrolyte (1.0 M $SBPBF_4$/ADN) at voltages up to 4.0 V.

As seen in Fig. 11a, the CV curves maintain a regular rectangular shape at operating voltages as high as 3.5 V or even 4.0 V. This indicates that the electrodes and electrolyte operate stably under high voltage conditions without undergoing chemical reactions. The maximum specific capacitance is calculated to be 164 F g^{-1}. The GCD curves in Fig. 11b have the form of nearly perfect isosceles triangles without significant distortion or plateau formation. Thus, the electrodes have an ideal electrical double-layer capacitor behavior. As shown in Fig. 11c, the elevated operating voltage and specific capacitance

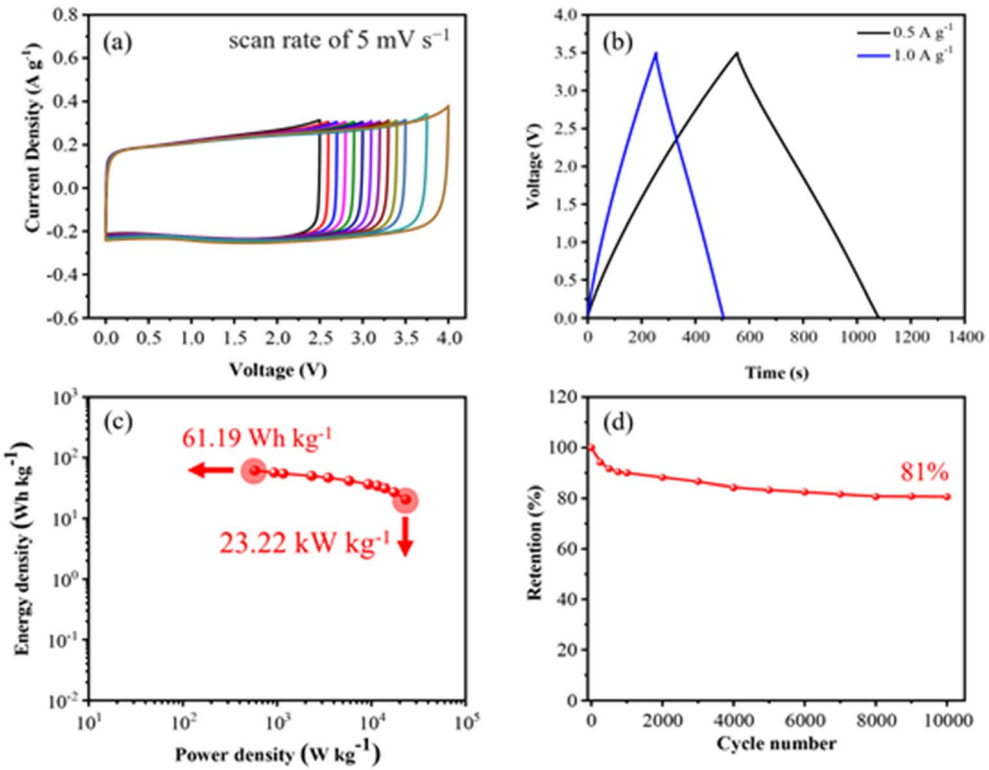

Fig. 11 Electrochemical performance of N-GMPC in 1.0 M $SBPBF_4$/ADN electrolyte during 10 000 cycles at a current density of 1.0 A g^{-1}. (a) CV curves. (b) GCD curves. (c) Ragone plot. (d) Cycling stability.

result in a high energy and power density (energy density: 61.19 W h kg^{-1}, power density: 23.22 kW kg^{-1}).

A 10 000-cycle life test was conducted in the voltage range of 3.0 to 3.5 V, the region most prone to electrolyte degradation.[58] The results in Fig. 11d confirm that, even under high-voltage conditions, the capacitance retention rate remains above 80% after 10 000 cycles at a current density of 1 A g^{-1}. This superior performance can be attributed to the nitrogen doping and high degree of graphitization of the N-GMPC material, which reduces potential side reactions in the electrolyte or electrode and provides excellent conductivity to mitigate the exothermic effects of the charge–discharge cycles.[59,60]

In summary, this novel synthesis method enhances the electrochemical performance of nitrogen-doped carbon through the following approaches: (1) formation of a porous structure: This method employs physical and chemical activation techniques to create N-GMPC with a 3D interconnected porous structure. Compared to untreated biochar, the specific surface area and pore volume of N-GMPC increase significantly. The high specific surface area provides more active sites for ion adsorption and desorption, thereby improving electrochemical performance. (2) Introduction of nitrogen doping: during the synthesis process, melamine and oyster shell powder are used as nitrogen sources, successfully incorporating nitrogen into the carbon material. Nitrogen doping enhances the conductivity of the carbon material and suppresses side reactions of the electrolyte or electrodes during charge–discharge processes, thereby extending the cycle life of the supercapacitor. (3) Improvement of graphitization degree: in the high-temperature (900 °C) activation process, the activator (KOH) reacts with the carbon, promoting the formation of long-range graphite structures and enhancing the degree of graphitization. A higher degree of graphitization improves the material's conductivity, facilitating rapid charge transport. (4) Enhancement of conductivity: nitrogen doping and a high degree of graphitization together enhance the conductivity of N-GMPC. DFT calculations confirm that the energy gap of N-GMPC is smaller than that of the original biochar, indicating easier charge transfer, which further improves electrochemical performance. This novel synthesis method effectively enhances the electrochemical performance of nitrogen-doped carbon by creating a porous structure, introducing nitrogen doping, improving the degree of graphitization, and enhancing conductivity. These improvements make it an ideal candidate as an electrode material for supercapacitors.

4. Conclusion

This study has presented a simple blending method for the one-pot synthesis of high-quality N-GMPC from wood-derived biowaste and oyster shell powder. The proposed method is environmentally friendly, straightforward, and applicable to various carbon sources. The synthesized N-GMPC material has many favorable characteristics for supercapacitor electrode materials, including a well-developed pore structure, high nitrogen content, and excellent graphitization. Its performance in supercapacitor applications is comparable to, or even better than, that of CPC in an organic electrolyte (1.0 M $TEABF_4$/PC). Furthermore, in a high-voltage electrolyte (1.0 M $SBPBF_4$/ADN), the N-GMPC demonstrates a high energy density (61.19 W h kg^{-1}) and power density (23.22 kW kg^{-1}), together with good cycling stability (81% capacitance retention after 10 000 cycles). Overall, the results suggest that the proposed synthesis process has significant potential for the commercial-scale conversion of waste wood biochar to high-value carbon materials.

Data availability

Data generated or analyzed during this study are fully provided within the published article and its ESI.†

Author contributions

Shu-Sian Wang: writing–original draft, methodology, investigation, data curation, conceptualization. Chun-Han Hsu: writing–review & editing, supervision, methodology, data curation. Cheng-Ta Tsai: data curation. Hong-Ping Lin: writing–review & editing, supervision, methodology, conceptualization. Che-Wei Yan: investigation, data curation. Jeng-Kuei Chang: supervision, methodology. Tzu-Hsien Hsieh & Cheng-Wei Huang & Cheng-Hsien Lee: validation, project administration.

Conflicts of interest

The authors declare that they have no known competing financial interests or personal relationships that could have appeared to influence the work reported in this paper.

Acknowledgements

This study was financially supported by the National Science and Technology Council (NSTC) of Taiwan. Additional funding was provided by the Hierarchical Green-Energy Materials (Hi-GEM) Research Center through the Featured Areas Research Center Program within the framework of the Higher Education Sprout Project of the Ministry of Education (MOE) in Taiwan. The authors gratefully acknowledge the access provided to JEOL JEM-2100F Cs STEM by the Core Facility Center of National Cheng Kung University, Tainan, Taiwan.

References

1 E. Hsu, Cost-benefit analysis for recycling of agricultural wastes in Taiwan, *Waste Manag.*, 2021, **120**, 424–432, DOI: 10.1016/j.wasman.2020.09.051.
2 J. Wang and S. Wang, Preparation, modification and environmental application of biochar: A review, *J. Cleaner Prod.*, 2019, **227**, 1002–1022, DOI: 10.1016/j.jclepro.2019.04.282.
3 C. Senthil and C. W. Lee, Biomass-derived biochar materials as sustainable energy sources for electrochemical energy storage devices, *Renewable Sustainable Energy Rev.*, 2021, **137**, 110464, DOI: 10.1016/j.rser.2020.110464.

4 R. P. Lopes and D. Astruc, Biochar as a support for nanocatalysts and other reagents: Recent advances and applications, *Coord. Chem. Rev.*, **426**, 213585, DOI: 10.1016/j.ccr.2020.213585.
5 M. I. Inyang, B. Gao, Y. Yao, Y. Xue, A. Zimmerman, A. Mosa, P. Pullammanappallil, Y. S. Ok and X. Cao, A review of biochar as a low-cost adsorbent for aqueous heavy metal removal, *Crit. Rev. Environ. Sci. Technol.*, 2016, **46**, 406–433, DOI: 10.1080/10643389.2015.1096880.
6 X. X. Guo, H. T. Liu and J. Zhang, The role of biochar in organic waste composting and soil improvement: A review, *Waste Manag.*, 2020, **102**, 884–899, DOI: 10.1016/j.wasman.2019.12.003.
7 G. Jiang, R. A. Senthil, Y. Sun, T. R. Kumar and J. Pan, Recent progress on porous carbon and its derivatives from plants as advanced electrode materials for supercapacitors, *J. Power Sources*, 2022, **520**, 230886, DOI: 10.1016/j.jpowsour.2021.230886.
8 J. Yin, W. Zhang, N. A. Alhebshi, N. Salah and H. N. Alshareef, Synthesis strategies of porous carbon for supercapacitor applications, *Small Methods*, 2020, **4**, 1900853, DOI: 10.1002/smtd.201900853.
9 R. Chakraborty, K. Vilya, M. Pradhan and A. K. Nayak, Recent advancement of biomass-derived porous carbon based materials for energy and environmental remediation applications, *J. Mater. Chem. A*, 2022, **10**, 6965–7005, DOI: 10.1039/D1TA10269A.
10 D. V. Cuong, B. M. Matsagar, M. Lee, Md. S. A. Hossain, Y. Yamauchi, M. Vithanage, B. Sarkar, Y. S. Ok, K. C. W. Wu and C. H. Hou, A critical review on biochar-based engineered hierarchical porous carbon for capacitive charge storage, *Renewable Sustainable Energy Rev.*, 2021, **145**, 111029, DOI: 10.1016/j.rser.2021.111029.
11 P. Wu, B. P. Singh, H. Wang, Z. Jia, Y. Wang and W. Chen, Bibliometric analysis of biochar research in 2021: a critical review for development, hotspots and trend directions, *Biochar*, 2023, **5**, 6, DOI: 10.1007/s42773-023-00204-2.
12 C. Zheng, X. Zhou, H. Gao, G. Wang and Z. Hu, Synthesis of porous graphene/activated carbon composite with high packing density and large specific surface area for supercapacitor electrode material, *J. Power Sources*, 2014, **258**, 290–296, DOI: 10.1016/j.jpowsour.2014.01.056.
13 X. Zhang, R. Han, Y. Liu, H. Li, W. Shi, X. Yan, X. Zhao, Y. Li and B. Liu, Porous and graphitic structure optimization of biomass-based carbon materials from 0D to 3D for supercapacitors: A review, *Chem. Eng. J.*, 2023, **460**, 141607, DOI: 10.1016/j.cej.2023.141607.
14 Z. Li, D. Guo, Y. Liu, H. Wang and L. Wang, Recent advances and challenges in biomass-derived porous carbon nanomaterials for supercapacitors, *Chem. Eng. J.*, 2020, **397**, 125418, DOI: 10.1016/j.cej.2020.125418.
15 W. Raza, F. Ali, N. Raza, Y. Luo, K. H. Kim, J. Yang, S. Kumar, A. Mehmood and E. E. Kwon, Recent advancements in supercapacitor technology, *Nano Energy*, 2018, **52**, 441–473, DOI: 10.1016/j.nanoen.2018.08.013.
16 M. Barczak and T. J. Bandosz, Evaluation of nitrogen- and sulfur-doped porous carbon textiles as electrode materials for flexible supercapacitors, *Electrochim. Acta*, 2019, **305**, 125–136, DOI: 10.1016/j.electacta.2019.03.014.
17 Y. Gong, D. Li, Q. Fu, Y. Zhang and C. Pan, Nitrogen self-doped porous carbon for high-performance supercapacitors, *ACS Appl. Energy Mater.*, 2020, **3**, 1585–1592, DOI: 10.1021/acsaem.9b02077.
18 B. M. Matsagar, R. X. Yang, S. Dutta, Y. S. OK and K. C. W. Wu, Recent progress in the development of biomass-derived nitrogen-doped porous carbon, *J. Mater. Chem. A*, 2021, **9**, 3703–3728, DOI: 10.1039/D0TA09706C.
19 F. Sun, D. Wu, J. Gao, T. Pei, Y. Chen, K. Wang, H. Yang and G. Zhao, Graphitic porous carbon with multiple structural merits for high-performance organic supercapacitor, *J. Power Sources*, 2020, **477**, 228759, DOI: 10.1016/j.jpowsour.2020.228759.
20 J. Maruyama, S. Maruyama, T. Fukuhara, K. Chashiro and H. Uyama, Ordered mesoporous structure by graphitized carbon nanowall assembly, *Carbon*, 2018, **126**, 452–455, DOI: 10.1016/j.carbon.2017.10.029.
21 J. Liu, Y. Liu, H. B. Zhang, Y. Dai, Z. Liu and Z. Z. Yu, Superelastic and multifunctional graphene-based aerogels by interfacial reinforcement with graphitized carbon at high temperatures, *Carbon*, 2018, **132**, 95–103, DOI: 10.1016/j.carbon.2018.02.026.
22 B. Yan, J. Zheng, L. Feng, Q. Zhang, C. Zhang, Y. Ding, J. Han, S. Jiang and S. He, Pore engineering: Structure-capacitance correlations for biomass-derived porous carbon materials, *Mater. Des.*, 2023, **229**, 111904, DOI: 10.1016/j.matdes.2023.111904.
23 L. Chuenchom, R. Kraehnert and B. M. Smarsly, Recent progress in soft-templating of porous carbon materials, *Soft Matter*, 2012, **8**, 10801–10812, DOI: 10.1039/C2SM07448F.
24 C. H. Hsu, Z. B. Pan, C. R. Chen, M. X. Wei, C. A. Chen, H. P. Lin and C. H. Hsu, Synthesis of multiporous carbons from the water caltrop shell for high-performance supercapacitors, *ACS Omega*, 2020, **5**, 10626–10632, DOI: 10.1021/acsomega.0c01212.
25 L. Wang, G. Mu, C. Tian, L. Sun, W. Zhou, P. Yu, J. Yin and H. Fu, Porous graphitic carbon nanosheets derived from cornstalk biomass for advanced supercapacitors, *ChemSusChem*, 2013, **6**, 880–889, DOI: 10.1002/cssc.201200990.
26 A. C. Ferrari and D. M. Basko, Raman spectroscopy as a versatile tool for studying the properties of graphene, *Nat. Nanotechnol.*, 2013, **8**, 235–246, DOI: 10.1038/nnano.2013.46.
27 S. Huo, Y. Zhao, M. Zong, B. Liang, X. Zhang, I. U. Khan, X. Song and K. Li, Boosting supercapacitor and capacitive deionization performance of hierarchically porous carbon by polar surface and structural engineering, *J. Mater. Chem. A*, 2020, **8**, 2505–2517, DOI: 10.1039/C9TA12170F.
28 P. Dai, S. Zhang, H. Liu, L. Yan, X. Gu, L. Li, D. Liu and X. Zhao, Cotton fabrics-derived flexible nitrogen-doped activated carbon cloth for high-performance supercapacitors in organic electrolyte, *Electrochim. Acta*, 2020, **354**, 136717, DOI: 10.1016/j.electacta.2020.136717.

29 J. Zhaong, C. Zhang, Y. Zhao, I. S. Amiinu, H. Zhou, X. Liu, Y. Tang and S. Mu, Three dimensional few-layer porous carbon nanosheets towards oxygen reduction, *Appl. Catal., B*, 2017, **211**, 148–156, DOI: 10.1016/j.apcatb.2017.04.038.

30 L. Xie, F. Su, L. Xie, X. Guo, Z. Wang, Q. Kong, G. Sun, A. Ahmad, X. Li, Z. Yi and C. Chen, Effect of pore structure and doping species on charge storage mechanisms in porous carbon-based supercapacitors, *Mater. Chem. Front.*, 2020, **4**, 2610–2634, DOI: 10.1039/d0qm00180e.

31 L. Cançado, K. Takai, T. Enoki, M. Endo, Y. A. Kim, H. Mizusaki, N. L. Spezialim, A. Jorio and M. A. Pimenta, Measuring the degree of stacking order in graphite by Raman spectroscopy, *Carbon*, 2008, **46**, 272–275, DOI: 10.1016/j.carbon.2007.11.015.

32 J. Xia, N. Zhang, S. Chong, De. Li, Y. Chen and C. Sun, Three-dimensional porous graphene-like sheets synthesized from biocarbon *via* low-temperature graphitization for a supercapacitor, *Green Chem.*, 2018, **20**, 694–700, DOI: 10.1039/c7gc03426a.

33 D. Liu, B. Xu, J. Zhu, S. Tang, F. Xu, S. Li, B. Jia and G. Chen, Preparation of highly porous graphitic activated carbon as electrode materials for supercapacitors by hydrothermal pretreatment-assisted chemical activation, *ACS Omega*, 2020, **5**, 11058–11067, DOI: 10.1021/acsomega.0c00938.

34 L. Dai, Q. Lu, H. Zhou, F. Shen, Z. Liu, W. Zhu and H. Huang, Tuning oxygenated functional groups on biochar for water pollution control: A critical review, *J. Hazard. Mater.*, 2021, **420**, 126547, DOI: 10.1016/j.jhazmat.2021.126547.

35 J. Wang and S. Kaskel, KOH activation of carbon-based materials for energy storage, *J. Mater. Chem.*, 2012, **45**, 23710–23725, DOI: 10.1039/c2jm34066f.

36 K. Nanaji, B. V. Sarada, U. V. Varadaraju, T. N Rao and S. Anandan, A novel approach to synthesize porous graphene sheets by exploring KOH as pore inducing agent as well as a catalyst for supercapacitors with ultra-fast rate capability, *Renewable Energy*, 2021, **172**, 502–513, DOI: 10.1016/j.renene.2021.03.039.

37 C. Wang, D. Li, T. Zhai, H. Wang, Q. Sun and H. Li, Direct conversion of waste tires into three-dimensional graphene, *Energy Storage Mater.*, 2019, **23**, 499–507, DOI: 10.1016/j.ensm.2019.04.014.

38 J. Zhang, Z. Xia and L. Dai, Carbon-based electrocatalysts for advanced energy conversion and storage, *Sci. Adv.*, 2015, **1**, e1500564, DOI: 10.1126/sciadv.1500564.

39 M. Ayiania, M. Smith, A. J. R. Hensley, L. Scudiero, J.-S. McEwen and M. Garcia-Perez, Deconvoluting the XPS spectra for nitrogen-doped chars: An analysis from first principles, *Carbon*, 2020, **162**, 528e544, DOI: 10.1016/j.carbon.2020.02.065.

40 G. Kharel, O. Sacko, X. Feng, J. R. Morris, C. L. Phillips, K. Trippe, S. Kumar and J. W. Lee, Biochar Surface oxygenation by ozonization for super high cation exchange capacity, *ACS Sustainable Chem. Eng.*, 2019, **7**, 16410–16418, DOI: 10.1021/acssuschemeng.9b03536.

41 K. Kaur, R. Kaur and H. Kaur, A systematic review of lignocellulosic biomass for remediation of environmental pollutants, *Appl. Surf. Sci.*, 2024, **19**, 100547, DOI: 10.1016/j.apsadv.2023.100547.

42 S. H. Ho, Y. D. Chen, R. Li, C. Zhang, Y. Ge, G. Cao, M. Ma, X. Duan, S. W and N. Q. Ren, N-doped graphitic biochars from C-phycocyanin extracted Spirulina residue for catalytic persulfate activation toward nonradical disinfection and organic oxidation, *Water Res.*, 2019, **159**, 77–86, DOI: 10.1016/j.watres.2019.05.008.

43 D. Guo, J. Qian, R. Xin, Z. Zhang, W. Jiang, G. Hu and M. Fan, Facile synthesis of nitrogen-enriched nanoporous carbon materials for high performance supercapacitors, *J. Colloid Interface Sci.*, 2019, **538**, 199–208, DOI: 10.1016/j.jcis.2018.11.107.

44 S. O. Adio, S. A. Ganiyu, M. Usman, I. Abdulazeez and K. Alhooshani, Facile and efficient nitrogen modified porous carbon derived from sugarcane bagasse for CO_2 capture: Experimental and DFT investigation of nitrogen atoms on carbon frameworks, *Chem. Eng. J.*, 2020, **382**, 122964, DOI: 10.1016/j.cej.2019.122964.

45 Y. Wang, Y. Song and Y. Xia, Electrochemical capacitors: mechanism, materials, systems, characterization and applications, *Chem. Soc. Rev.*, 2016, **21**, 5925–5950, DOI: 10.1039/c5cs00580a.

46 B. A. Mei, O. Munteshari, J. Lau, B. Dunn and L. Pilon, Physical interpretations of Nyquist plots for EDLC electrodes and devices, *J. Phys. Chem. C*, 2018, **122**, 194–206, DOI: 10.1021/acs.jpcc.7b10582.

47 M. Y. Perdana, B. A. Johan, M. Abdallah, M. E. Hossain, M. A. Aziz, T. N. Baroud and Q. A. Drmosh, Understanding the behavior of supercapacitor materials *via* electrochemical impedance spectroscopy: A review, *Chem. Rec.*, 2024, **24**, e202400007, DOI: 10.1002/tcr.202400007.

48 B. Wang, X. Wu, Y. Yu, N. Wang and Z. Zhou, Simultaneously tuning the hierarchical porous structure and graphitization degree of biomass derived carbon for supercapacitors, *Electrochim. Acta*, 2022, **432**, 141219, DOI: 10.1016/j.electacta.2022.141219.

49 B. Gang, F. Zhang, X. Li, B. Zhai, X. Wang and Y. Song, A ulva lactuca-derived porous carbon for high-performance electrode materials in supercapacitor: Synergistic effect of porous structure and graphitization degree, *J. Energy Storage*, 2021, **33**, 102132, DOI: 10.1016/j.est.2020.102132.

50 N. Jäckel, D. Weingarth, A. Schreiber, B. Kruner, M. Zeiger, A. Tolosa, M. Aslan and V. Presser, Performance evaluation of conductive additives for activated carbon supercapacitors in organic electrolyte, *Electrochim. Acta*, 2016, **191**, 284–298, DOI: 10.1016/j.electacta.2016.01.065.

51 R. Na, N. Li, L. Li, Y. Liu, J. Luan and G. Wang, A robust conductive polymer network as a multi-functional binder and conductive additive for supercapacitors, *Chemelectrochem*, 2020, **7**, 3056–3064, DOI: 10.1002/celc.202000726.

52 P. Wang, X. Qi, W. Zhao, M. Qian, H. Bi and F. Huang, Nitrogen-doped hierarchical few-layered porous carbon for efficient electrochemical energy storage, *Carbon Energy*, 2021, **3**, 349–359, DOI: 10.1002/cey2.78.

53 J. He, D. Zhang, Y. Wang, J. Zhang, B. Yang, H. Shi, K. Wang and Y. Wang, Biomass-derived porous carbons with tailored graphitization degree and pore size distribution for supercapacitors with ultra-high rate capability, *Appl. Surf. Sci.*, 2020, **515**, 146020, DOI: 10.1016/j.apsusc.2020.146020.

54 S. Sutarsis, J. Patra, C. Y. Su, J. Li, D. Bresser, S. Passerini and J. K. Chang, Manipulation of nitrogen-heteroatom configuration for enhanced charge-storage performance and reliability of nanoporous carbon electrodes, *ACS Appl. Mater. Interfaces*, 2020, **12**, 32797–32805, DOI: 10.1021/acsami.0c08440.

55 X. Y. Chen, C. Chen, Z. J. Zhang, D. H. Xie, X. Deng and J. W. Liu, Nitrogen-doped porous carbon for supercapacitor with long-term electrochemical stability, *J. Power Sources*, 2013, **230**, 50–58, DOI: 10.1016/j.jpowsour.2012.12.054.

56 B. Zhang, F. Sun, Y. Li, D. Wu, C. Yang, Z. Wang, J. Gao, G. Zhao and S. Sun, Changing the potassium-based activation path to prepare coal-based porous carbon with more graphitic or graphene structures for high-performance organic supercapacitors, *Carbon*, 2024, **219**, 118812, DOI: 10.1016/j.carbon.2024.118812.

57 T. S. Bhat, P. S. Patil and R. B. Rakhi, Recent trends in electrolytes for supercapacitors, *J. Energy Storage*, 2022, **50**, 104222, DOI: 10.1016/j.est.2022.104222.

58 J. M. Lim, Y. S. Jang, H. V. T. Nguyen, J. S. Kim, Y. Yoon, B. J. Park, D. H. Seo, K. K. Lee, Z. Han, K. Ostrikov and S. G. Doo, Advances in high-voltage supercapacitors for energy storage systems: materials and electrolyte tailoring to implementation, *Nanoscale Adv.*, 2023, **5**, 615–626, DOI: 10.1039/D2NA00863G.

59 D. Gandla, X. Wu, F. Zhang, C. Wu and D. Q. Tan, High-performance and high-voltage supercapacitors based on N-doped mesoporous activated carbon derived from dragon fruit peels, *ACS Omega*, 2021, **6**, 7615–7625, DOI: 10.1021/acsomega.0c06171.

60 A. Likitchatchawankun, A. Kundu, O. Munteshari, T. Fisher and L. Pilon, Heat generation in all-solid-state supercapacitors with graphene electrodes and gel electrolytes, *Electrochim. Acta*, 2019, **303**, 341–353, DOI: 10.1016/j.electacta.2019.02.031.

